Available online at www.sciencedirect.com
ScienceDirect
International Journal of Heat and Mass Transfer 50 (2007) 3521–3533
International Journal of HEAT and MASS TRANSFER
www.elsevier.com/locate/ijhmt

Thermally developing Brinkman–Brinkman forced convection in rectangular ducts with isothermal walls

K. Hooman [a,*], A. Haji-Sheikh [b], D.A. Nield [c]

[a] School of Engineering, The University of Queensland, Brisbane, Australia
[b] Department of Mechanical and Aerospace Engineering, The University of Texas at Arlington, 500 W. First Street, Arlington, TX 76019-0023, USA
[c] Department of Engineering Science, University of Auckland, Private Bag 92019, Auckland, New Zealand

Received 22 July 2006; received in revised form 6 January 2007
Available online 26 March 2007

Abstract

The Extended Weighted Residuals Method (EWRM) is applied to investigate the effects of viscous dissipation on the thermal development of forced convection in a porous-saturated duct of rectangular cross-section with isothermal boundary condition. The Brinkman flow model is employed for determination of the velocity field. The temperature in the flow field was computed by utilizing the Green's function solution based on the EWRM. Following the computation of the temperature field, expressions are presented for the local Nusselt number and the bulk temperature as a function of the dimensionless longitudinal coordinate. In addition to the aspect ratio, the other parameters included in this computation are the Darcy number, viscosity ratio, and the Brinkman number.

Keywords: Extended Weighted Residuals Method; Porous media; Viscous dissipation; Thermal development; Rectangular duct; Brinkman–Brinkman problem

1. Introduction

Flow through porous media is important in numerous engineering applications including geothermal energy, petroleum reservoirs, nuclear reactors, drying, and fuel cells. Almost all of the natural porous media are associated with such small porosity that the Darcy flow model is applicable. However, for man-made porous media with higher porosity, the Brinkman model predicts hydraulics through such hyperporous media, as noted by Nield and Bejan [1].

Because of the use of the so-called hyperporous media in the cooling of electronic equipment, there has recently been renewed interest in the problem of forced convection in a porous medium channel. However, the literature on the effects of viscous dissipation on thermal development is limited to work pertaining to parallel plate channel [2–5] or circular tube [6–9]. In some of these articles the velocity distribution is slug type while in others the boundary and shear effects are included via a Brinkman term to form a Brinkman–Brinkman problem. The term 'Brinkman–Brinkman', proposed by Nield [10], refers to a problem involving a saturated porous medium in which the momentum transfer is modeled by a Brinkman equation [11], and the thermal energy equation includes a viscous dissipation term involving a Brinkman number [12]. The problem becomes more complicated when one seeks analytical solutions for a thermally developing Brinkman–Brinkman problem through ducts of arbitrary cross-section. For two-dimensional ducts, the complexity of the problems become clearer when one observes that even fully developed solutions, with or without the effects of viscous dissipation, are limited to the work reported in [13–16]. The studies of the thermally developing forced convection heat transfer in elliptical ducts in [17] and for ducts with rectangular cross-sections [18] are without inclusion of the

* Corresponding author. Tel.: +61 7 33653668; fax: +61 7 33654799.
E-mail address: k.hooman@uq.edu.au (K. Hooman).

0017-9310/$ - see front matter © 2007 Elsevier Ltd. All rights reserved.
doi:10.1016/j.ijheatmasstransfer.2007.01.011

Nomenclature

A	area (m^2)
A	matrix
a	duct dimension, see Fig. 1
a_{ij}	elements of matrix **A**
B	matrix
B_m	coefficients
b	duct dimension, see Fig. 1
b_{ij}	elements of matrix **B**
Br	Brinkman number, $\mu_e U^2/[k_e(T_1 - T_2)]$
c_p	constant pressure specific heat (J/kg K)
D	matrix
Da	Darcy number (K/a^2)
D_h	hydraulic diameter $4ab/(a+b)$ (m)
d_{mj}	elements of matrix **D**
E	matrix with elements e_{ij}
e_{ij}	elements of matrix **E**
f_i, f_j	basis functions
G	Green's function
h	heat transfer coefficient (W/m^2 K)
$\bar{h}$	average heat transfer coefficient (W/m^2 K)
i, j	indices
K	permeability (m^2)
k_e	effective thermal conductivity (W/m K)
M	viscosity ratio, μ_e/μ
m, n	indices
Nu_D	local Nusselt number, hD_h/k_e
$\bar{N}u_D$	average Nusselt number, $\bar{h}D_h/k_e$
P	matrix having elements p_{mi}
Pe	Péclet number, $\rho c_p U a/k_e$
Pr	Prandtl number, $\mu_e c_p/k_e$
p	pressure (Pa)
p_{mi}	elements of matrix **P**
Re_D	Reynolds number, $\rho U D_h/\mu_e$
S	volumetric heat source, Eq. (4b) (W/m^3)
S^*	dimensionless heat source, Eq. (18b)
T	temperature (K)
T_1	temperature at $x = 0$ (K)
T_2	wall temperature (K)
U	average velocity (m/s)
u	velocity (m/s)
$\bar{u}$	dimensionless velocity, $-\mu u/(a^2 \partial p/\partial x)$
$\hat{u}$	u/U
x	axial coordinate (m)
$\bar{x}$	$(x/a)/Pe$
y, z	coordinates (m)
$\bar{y}, \bar{z}$	y/a and z/a

Greek symbols

θ	dimensionless temperature
λ_m	eigenvalues
μ	fluid viscosity (N s/m^2)
μ_e	effective viscosity (N s/m^2)
ξ	dummy variable of integration
ρ	fluid density (kg/m^3)
ψ	eigenfunction

Subscripts

b	bulk
e	effective
o	unheated length
w	wall

viscous dissipation effects. In a recent work, Haji-Sheikh et al. [19] have considered the effects of viscous dissipation on heat transfer in the entrance region of ducts of arbitrary cross-section with a special attention to the isosceles triangular case.

Earlier work on the effects of viscous dissipation in ducts, clear of solid material, is surveyed by Shah and London [20] and for in porous media surveyed by Magyari et al. [22]. This paper treats the more general case of thermally developing forced convection in rectangular ducts wherein the viscous dissipation is significant. The EWRM in an extended form, as discussed in [19], is the selected computational methodology. This study treats the case of a duct of rectangular cross-section with walls held at a constant and uniform temperature, i.e. the **T** boundary condition in the terminology of Shah and London [20], which is appropriate when the thermal conductivity of the enclosing walls is sufficiently high. Here, the Green's function solution in [18] is modified mainly to account for the viscous dissipation effects on the thermal development. For the case of the Darcy flow model, the hydrodynamically developed velocity profile is that of slug flow, and the problem is mathematically similar to a pure conduction [21], but this paper considers the more complicated flow appropriate to the Brinkman model.

2. Analysis

2.1. Fluid flow analysis

For a passage with a constant but arbitrarily shaped cross-section, based on the ligament dimension, the Brinkman momentum equation, is

$$\mu_e\left(\frac{\partial^2 u}{\partial y^2}+\frac{\partial^2 u}{\partial z^2}\right)-\frac{\mu}{K}u-\frac{\partial p}{\partial x}=0. \tag{1}$$

By selecting $\bar{y} = y/a$, $\bar{z} = z/a$, and $\bar{u} = -\mu u/(a^2 \partial p/\partial x)$, the dimensionless form of Eq. (1) becomes,

$$M\left(\frac{\partial^2 \bar{u}}{\partial \bar{y}^2}+\frac{\partial^2 \bar{u}}{\partial \bar{z}^2}\right)-\frac{1}{Da}\bar{u}+1=0, \tag{2}$$

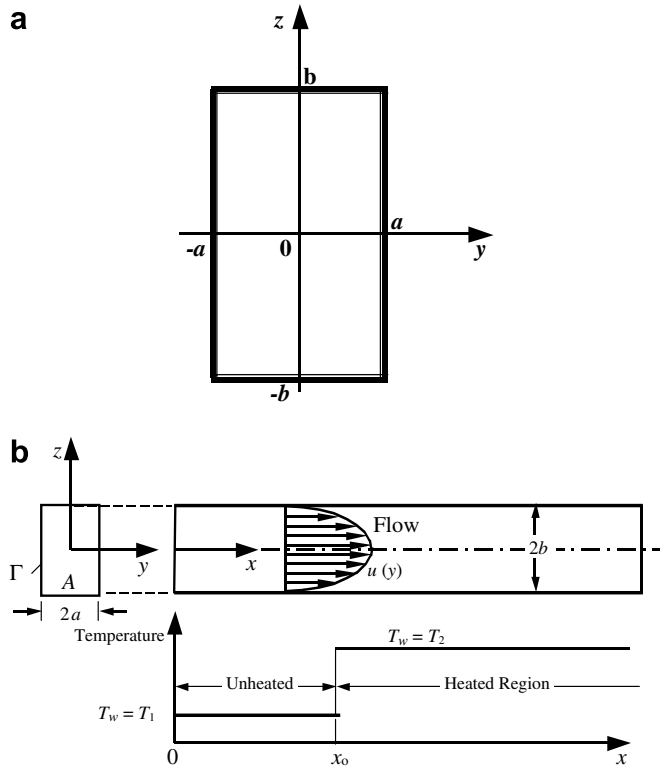

Fig. 1. Schematic of rectangular duct and the coordinated (a) cross-section and (b) the boundary conditions.

wherein $M = \mu_e/\mu$ and $Da = K/a^2$ is the Darcy number. Moreover, μ_e is the effective viscosity, μ is the fluid viscosity, K is the permeability, and a is an arbitrarily chosen length scale in Fig. 1a. Although the exact series solution to Eq. (2), subject to the boundary condition $\bar{u} = 0$ at the walls is known (see [14,16]), for convenience of subsequent computations, the solution is obtained using the variational calculus. Therefore, by definition, the mean velocity is

$$U = \frac{1}{A}\int_A u\,\mathrm{d}A \tag{3a}$$

and the normalized velocity is

$$\hat{u} = \frac{u}{U}. \tag{3b}$$

It is worth noting that A in Eq. (3a) is the cross-sectional area of the duct. The details related to the hydrodynamic aspects of the problem and the exact series solutions are in [14,16,18].

2.2. Heat transfer analysis

In this solution, the uniform inlet temperature T_1 remains constant and the wall temperature is fixed at the same temperature T_1 for a distance x_o. Then, at $x = x_o$, the wall temperature changes to a constant and locally uniform temperature T_2, see Fig. 1b. Throughout this calculation, the local thermal equilibrium assumption remains valid. Under steady-state condition and when the thermophysical properties are independent of temperature, the thermal energy equation for the fully developed and incompressible flow through the porous passage is

$$\frac{\partial}{\partial y}\left(k_e\frac{\partial T}{\partial y}\right) + \frac{\partial}{\partial z}\left(k_e\frac{\partial T}{\partial z}\right) + S(y,z;x) = \rho c_p u\frac{\partial T}{\partial x}, \tag{4a}$$

where

$$S(y,z) = \frac{\mu u^2}{K} + \mu_e\left[\left(\frac{\partial u}{\partial y}\right)^2 + \left(\frac{\partial u}{\partial z}\right)^2\right]. \tag{4b}$$

Eq. (4a) is valid if the Péclet number is sufficiently large so that the effects of axial conduction could be neglected.

To obtain the Green's function, it is preferred to solve Eq. (4a) in the absence of the frictional heating term. Once the Green's function is known, the Green's function solution would include the contributions of the frictional heating and non-uniform wall temperature. Now, in the absence of the source term, consider a temperature solution of the following form

$$T(y,z;x) = \Psi(y,z)\mathrm{e}^{-\lambda^2 x} \tag{5}$$

and the substitution of $T(y,z;x)$ from Eq. (5) in (4a) yields

$$\frac{\partial}{\partial y}\left(k_e\frac{\partial \Psi}{\partial y}\right) + \frac{\partial}{\partial z}\left(k_e\frac{\partial \Psi}{\partial z}\right) + \lambda^2\rho c_p u\Psi = 0. \tag{6}$$

The variational calculus requires the minimization of the functional [19]

$$I = \int_A \left\{k_e\left(\frac{\partial \Psi}{\partial y}\right)^2 + k_e\left(\frac{\partial \Psi}{\partial z}\right)^2 - \lambda^2\rho c_p u\Psi^2 - \frac{1}{2}\left[\frac{\partial}{\partial y}\left(k_e\frac{\partial \Psi^2}{\partial y}\right) + \frac{\partial}{\partial z}\left(k_e\frac{\partial \Psi^2}{\partial z}\right)\right]\right\}\mathrm{d}A, \tag{7}$$

when

$$\Psi = \sum_{j=1}^{N} d_j f_j(y,z) \tag{8}$$

and $f_j(y,z)$ functions, for $j = 1,2,\ldots,N$, are known as the basis functions. When the walls of a rectangular duct are located at $y = \pm a$ and $z = \pm b$, as shown in Fig. 1a, the following basis functions are selected

$$f_j = (a^2 - y^2)(b^2 - z^2)y^{2(m_j-1)}z^{2(n_j-1)} \tag{9}$$

using all combinations of $m_j = 1,2,\ldots$ and $n_j = 1,2,\ldots$ As required by this solution method, each of these basis functions vanishes at the wall.

The minimization of functional $I(d_1,d_2,\ldots,d_N)$ requires having

$$\frac{\partial I}{\partial d_i} = 0 \quad \text{for } i = 1,2,\ldots,N. \tag{10}$$

This leads to the relation

$$\sum_{j=1}^{N} d_j \left\{ \int_A \left[\frac{\partial}{\partial y}\left(k_e \frac{\partial f_j(y,z)}{\partial y} \right) + \frac{\partial}{\partial y}\left(k_e \frac{\partial f_j(y,z)}{\partial z} \right) \right] f_i \, dA + \lambda^2 \int_A \rho c_p u f_j f_i \right\} = 0 \quad \text{for } i = 1,2,\ldots,N, \tag{11}$$

that has the following matrix form,

$$(\mathbf{A} + \lambda^2 \mathbf{B}) \cdot \mathbf{d} = 0 \tag{12}$$

and wherein the matrices **A** and **B** have the members

$$a_{ij} = \int_A f_i(y,z) \nabla \cdot [k_e \nabla f_j(y,z)] dA = -\int_A k_e \nabla f_i(y,z) \cdot \nabla f_j(y,z) dA \tag{13a}$$

and

$$b_{ij} = \int_A \rho c_p u(y,z) f_i(y,z) f_j(y,z) dA. \tag{13b}$$

The matrices **A** and **B** are symmetric and the coefficients $(d_1, d_2, \ldots, d_N)$ in Eq. (8) are the members of a vector **d**. These coefficients and the eigenvalues are obtainable from the relation

$$(\mathbf{B}^{-1}\mathbf{A} + \lambda^2 \mathbf{I})\mathbf{d} = 0. \tag{14}$$

Once λ_m^2 and d_{mj} are known, the eigenfunction $\Psi_m(y,z)$, as defined in Eq. (8), becomes

$$\Psi_m(y,z) = \sum_{j=1}^{N} d_{mj} f_j(y,z) \tag{15}$$

for each eigenvalue (λ_m). The Green's function solution in a region whose boundary designated as Γ and it includes the contribution of frictional heating, as presented in [2,21], is

$$T(y,z;x) = \frac{1}{\rho c_p}\left\{ \int_{\xi=0}^{x} d\xi \int_{\Gamma} k_e \left(G \frac{\partial T}{\partial n} - T \frac{\partial G}{\partial n} \right)_{\Gamma'} d\Gamma' + \int_{\xi=0}^{x} d\xi \int_{z'=0}^{\bar{b}} \int_{y'=0}^{1} GS(y',z';\xi) dy' dz' + \int_{z'=0}^{\bar{b}} \int_{y'=0}^{1} \rho c_p u(y',z') G(y,z,x|y',z',0) T(y',z';0) dy' dz' \right\}, \tag{16a}$$

wherein the Green's function G stands for

$$G(y,z,x|y',z',\xi) = \sum_{m=1}^{N} \left[\sum_{i=1}^{N} p_{mi} f_i(y',z') \right] \Psi_m(y,z) e^{-\lambda_m^2 (x-\xi)} \tag{16b}$$

and p_{mi} are members of the matrix $\mathbf{P} = [(\mathbf{D} \cdot \mathbf{B})^{\mathrm{T}}]^{-1}$. Following the determination of the Green's function, the dimensionless temperature $\theta = (T - T_2)/(T_1 - T_2)$ replaces T in Eq. (16a) and its solution becomes obtainable. Accordingly, when boundary conditions are homogeneous the first term in Eq. (16a) vanishes and the temperature solution takes the following form

$$\theta(y,z;x) = \int_{z=0}^{\bar{b}} \int_{y=0}^{1} u(y',z') G(y,z,x|y',z',0) dy' dz' + \frac{1}{\rho c_p} \int_{\xi=0}^{x} d\xi \int_{z=0}^{\bar{b}} \int_{y=0}^{1} GS(y',z';\xi) dy' dz'. \tag{17}$$

The application of energy balance to a differential element located at location x, leads toward the computation of the Nusselt number. Using the dimensionless coordinates defined earlier and after setting $\bar{x} = (x/a)/Pe$ with $Pe = \rho c_p U a / k_e$, the local Nusselt number is

$$Nu_D = \left(\frac{D_h}{2a} \right)^2 \left\{ -\left[\frac{d\theta_b(\bar{x})/d\bar{x}}{\theta_b(\bar{x})} \right] + \left[\frac{Br}{\theta_b(\bar{x})} \right] \langle S^* \rangle \right\}, \tag{18a}$$

where $Br = \mu_e U^2/[k_e(T_1 - T_2)]$ and the function S^* includes the effect of frictional heating that, in the absence of any other volumetric heat source, takes the following form

$$S^* = \frac{\hat{u}^2}{MDa} + \left(\frac{\partial \hat{u}}{\partial \bar{y}} \right)^2 + \left(\frac{\partial \hat{u}}{\partial \bar{z}} \right)^2. \tag{18b}$$

Moreover, the angle brackets in Eq. (18a) denote an average taken over the duct cross-section as

$$\langle S^* \rangle = \frac{1}{1 \times \bar{b}} \int_{z=0}^{\bar{b}} \int_{y=0}^{1} \left[\frac{\hat{u}^2}{MDa} + \left(\frac{\partial \hat{u}}{\partial \bar{y}} \right)^2 + \left(\frac{\partial \hat{u}}{\partial \bar{z}} \right)^2 \right] d\bar{y} \, d\bar{z}. \tag{19a}$$

Similarly, by definition, the bulk temperature is

$$\theta_b(\bar{x}) = \langle \hat{u}\theta \rangle. \tag{19b}$$

In the formulation of Eq. (19a), the viscous dissipation model proposed by Al-Hadhrami et al. [23] is being used. For details on the alternative viscous dissipation models one may consult [22–32].

3. Solution procedure

As stated earlier, the velocity distribution is computed using the variational calculus as presented in [19]. Once the velocity field is known, the dimensionless thermal energy equation

$$\frac{\partial^2 \theta}{\partial \bar{y}^2} + \frac{\partial^2 \theta}{\partial \bar{z}^2} + BrS^* = \hat{u} \frac{\partial \theta}{\partial \bar{x}} \tag{20}$$

is to be solved subject to the boundary conditions as depicted in Fig. 1b. The dimensionless temperature has a unit value at $x = 0$. At the wall $\theta(\pm 1, \bar{z}; \bar{x}) = 1$ and $\theta(\bar{y}, \pm \bar{b}; \bar{x}) = 1$ when $0 \leqslant x < x_o$ while it maintains the symmetry conditions about $y = 0$ and $z = 0$. Meanwhile, at location $x = x_o$, the dimensionless wall temperature suffers a change and assumes a zero value; that is, $\theta(\pm 1, \bar{z}; \bar{x}) = \theta(\bar{y}, \pm \bar{b}; \bar{x}) = 0$.

For convenience of mathematical formulations, Eq. (20) and its boundary conditions are decomposed into two different partial differential equations. Accordingly, one can set

$$\theta(\bar{y},\bar{z};\bar{x}) = \theta_{\mathrm{w}}(\bar{y},\bar{z};\bar{x}) + \theta_s(\bar{y},\bar{z};\bar{x}) \tag{21}$$

in which the first solution $\theta_{\mathrm{w}}(\bar{y},\bar{z};\bar{x})$ must satisfy the following partial differential equation

$$\frac{\partial^2\theta_{\mathrm{w}}}{\partial\bar{y}^2} + \frac{\partial^2\theta_{\mathrm{w}}}{\partial\bar{z}^2} = \hat{u}\frac{\partial\theta_{\mathrm{w}}}{\partial\bar{x}}, \tag{22}$$

subject to conditions $\theta_{\mathrm{w}}(\bar{y},\bar{z};0) = 1$, $\theta_{\mathrm{w}}(\pm1,\bar{z};\bar{x}) = \theta_{\mathrm{w}}(\bar{y},\pm\bar{b};\bar{x}) = 1$ when $0 \leqslant \bar{x} < \bar{x}_{\mathrm{o}}$ while $\theta_{\mathrm{w}}(1,\bar{z};\bar{x}) = \theta_{\mathrm{w}}(\bar{y},\bar{b};\bar{x}) = 0$ when $\bar{x} \geqslant 0$, and the condition of symmetry at $\bar{y} = 0$ and $\bar{z} = 0$. Next, the second solution $\theta_s(\bar{y},\bar{z};\bar{x})$ must satisfy the following partial differential equation

$$\frac{\partial^2\theta_s}{\partial\bar{y}^2} + \frac{\partial^2\theta_s}{\partial\bar{z}^2} + BrS^* = \hat{u}\frac{\partial\theta_s}{\partial\bar{x}}, \tag{23}$$

with boundary conditions $\theta_s(\bar{y},\bar{z};0) = \theta_s(1,\bar{z};\bar{x}) = \theta_s(\bar{y},\bar{b};\bar{x}) = 0$, and the condition of symmetry at $\bar{y} = 0$ and $\bar{z} = 0$.

Based on the specified boundary conditions, $\theta_{\mathrm{w}}(\bar{y},\bar{z};\bar{x}) = 1$ is the solution when $\bar{x} \leqslant \bar{x}_{\mathrm{o}}$. The Green's function solution for $\theta_{\mathrm{w}}(\bar{y},\bar{z};\bar{x})$, when $\bar{x} > \bar{x}_{\mathrm{o}}$, is

$$\theta_{\mathrm{w}}(\bar{y},\bar{z};\bar{x}) = \int_{z'=0}^{\bar{b}}\int_{y'=0}^{1}\hat{u}(y',z')\sum_{m=1}^{N}\left[\sum_{i=1}^{N}p_{mi}f_i(y',z')\right] \times \Psi_m(\bar{y},\bar{z})\mathrm{e}^{-\lambda_m^2(\bar{x}-\bar{x}_{\mathrm{o}})}\mathrm{d}y'\,\mathrm{d}z' \tag{24}$$

and the Nusselt number is being defined as

$$Nu_{D,\mathrm{w}} = -\frac{1}{4\theta_{\mathrm{b,w}}}\frac{\mathrm{d}\theta_{\mathrm{b,w}}}{\mathrm{d}\bar{x}}. \tag{25}$$

Moreover, the Green's function solution for $\theta_s(\bar{y},\bar{z};\bar{x})$ is

$$\theta_s(\bar{y},\bar{z};\bar{x}) = Br\int_{\xi=0}^{\bar{x}}\mathrm{d}\xi\int_{z'=0}^{\bar{b}}\int_{y'=0}^{1}\sum_{m=1}^{N}\left[\sum_{i=1}^{N}p_{mi}f_i(y',z')\right] \times \Psi_m(\bar{y},\bar{z})\mathrm{e}^{-\lambda_m^2(\bar{x}-\xi)}S^*(y',z';\xi)\mathrm{d}y'\,\mathrm{d}z'. \tag{26}$$

For this case the Nusselt number is defined as

$$Nu_{D,\mathrm{s}} = \left(\frac{D_{\mathrm{h}}}{2a}\right)^2\frac{\langle S^*\rangle - \mathrm{d}(\theta_{\mathrm{b,s}}/Br)/\mathrm{d}\bar{x}}{\theta_{\mathrm{b,s}}/Br}. \tag{27}$$

In this formulation, the dimensionless temperature is decomposed into these two contributions and this is done for some physical reason as well as the mathematical ones. These two solutions have interesting physical interpretation. The first solution called $\theta_{\mathrm{w}}(\bar{y},\bar{z};\bar{x})$ does not include the frictional heating effects. It can be interpreted as a problem for which the fluid enters the duct at a temperature the same as that of the walls, and then, at a distance x_{o} away from entrance location, the wall temperature abruptly changes. For this case, the results for $x \geqslant x_{\mathrm{o}}$ are similar to those in [18].

The second solution simulates a problem for which the wall temperatures remain at a constant value and the fluid enters the duct at a temperature equal to temperature at the walls. The main reason for transfer of heat to the walls is the internal heating induced by viscous dissipation. Accordingly, the temperature in the absence of a wall temperature change, when $\theta_{\mathrm{w}}(\bar{y},\bar{z};\bar{x}) = 0$ in Eq. (21), or when $0 \leqslant \bar{x} < \bar{x}_{\mathrm{o}}$ is obtainable from the relation

$$\frac{T - T_2}{T_1 - T_2} = 1 + \theta_s(\bar{y},\bar{z}:\bar{x}) = 1 + \frac{\mu_{\mathrm{e}}U^2}{k_{\mathrm{e}}(T_1 - T_2)}\left[\frac{\theta_s(\bar{y},\bar{z}:\bar{x})}{Br}\right], \tag{28a}$$

that reduces to

$$T = T_1 + \frac{\mu_{\mathrm{e}}U^2}{k_{\mathrm{e}}}\left[\frac{\theta_s(\bar{y},\bar{z}:\bar{x})}{Br}\right], \tag{28b}$$

without direct effect of any arbitrarily selected T_2. Tables 1–4 are prepared to provide the developing region bulk temperature $\langle\theta_s(\bar{y},\bar{z}:\bar{x})\rangle/Br$, related to the term within square brackets, for the aspect ratios b/a =1, 2, 4, and 10 while MDa is being a parameter. These tables also include the corresponding value of $Nu_{D,\mathrm{s}}$ for the same variables. For completeness, the dimensionless bulk temperature $\theta_{\mathrm{w}}(\bar{y},\bar{z}:\bar{x})$ and the Nusselt number $Nu_{D,\mathrm{w}}$ due to the wall effects are included in the following columns. This permits the determination of the combined effect using the relation

$$Nu_D(\bar{x}) = \frac{Nu_{D,\mathrm{w}}(\bar{x}-\bar{x}_{\mathrm{o}})\theta_{\mathrm{b,w}}(\bar{x}-\bar{x}_{\mathrm{o}}) + \theta_{\mathrm{b,s}}(\bar{x})Nu_{D,\mathrm{s}}(\bar{x})}{\theta_{\mathrm{b,w}}(\bar{x}-\bar{x}_{\mathrm{o}}) + \theta_{\mathrm{b,s}}(\bar{x})} \tag{29}$$

for a broad range of parameters when $\bar{x} > \bar{x}_{\mathrm{o}}$. The quantity $Nu_{D,\mathrm{s}}(\bar{x})$ is directly obtainable from data appearing in Tables 1–4; however, in order to get the $\theta_{\mathrm{b,s}}(\bar{x})$ value, one should multiply Br by the quantity $\theta_{\mathrm{b,s}}(\bar{x})/Br$. If the wall temperature T_2 appears at $\bar{x}_{\mathrm{o}} = 0$, these tables directly provide the quantities $\theta_{\mathrm{b,w}}(\bar{x})$ and $Nu_{D,\mathrm{w}}(\bar{x})$, in Eq. (29); however, when $\bar{x}_{\mathrm{o}} > 0$, the tabulated data for $\bar{x}$ stand for those for $(\bar{x}-\bar{x}_{\mathrm{o}})$. Additionally, the numerator of Eq. (29) represents the dimensionless local wall heat flux entering the medium,

$$\frac{[q_{\mathrm{w}}(\bar{x})]_{in}D_{\mathrm{h}}}{k_{\mathrm{e}}(T_2 - T_1)} = Nu_{D,\mathrm{w}}(\bar{x}-\bar{x}_{\mathrm{o}})\theta_{\mathrm{b,w}}(\bar{x}-\bar{x}_{\mathrm{o}}) + \theta_{\mathrm{b,s}}(\bar{x})Nu_{D,\mathrm{s}}(\bar{x}) = \left(\frac{D_{\mathrm{h}}}{2a}\right)^2\left(-\frac{\mathrm{d}\theta_b}{\mathrm{d}\bar{x}} + Br\langle S^*\rangle\right), \tag{30}$$

whose integration would yield the total heat flux within any $\bar{x}$ increment.

As an illustration, for b/a =4, $MDa = 0.01$, and $\bar{x}_{\mathrm{o}}$ being sufficiently large, Table 3b gives $Nu_{D,\mathrm{s}} = 7.59$ and $\theta_{\mathrm{b,s}}/Br = 38.39$, Eq. (29) yields the Nusselt number

$$Nu_D(\bar{x}-\bar{x}_{\mathrm{o}}) = \frac{Nu_{D,\mathrm{w}}(\bar{x}-\bar{x}_{\mathrm{o}})\theta_{\mathrm{b,w}}(\bar{x}-\bar{x}_{\mathrm{o}}) + 38.39\times 7.59Br}{\theta_{\mathrm{b,w}}(\bar{x}-\bar{x}_{\mathrm{o}}) + 38.39Br}. \tag{31}$$

This considers the first column in Table 3b to be $(\bar{x}-\bar{x}_{\mathrm{o}})$.

For different aspect ratios, Tables 1–4 include a summary of the data, acquired for individual contributions, as a function of $\bar{x}$ for different values of the parameter MDa. Also, data are plotted in Figs. 2–4 mainly to illustrate the general behavior of these data. The results for the combined effects are plotted in Figs. 5–8. The data in

Table 1
The bulk temperatures and the Nusselt numbers when $b/a = 1$, for (a) $MDa = \infty$ and 1, (b) $MDa = 0.1$ and 0.01, and (c) $MDa = 0.001$ and 0.0001

$\frac{x/a}{Pe}$	$MDa = \infty$				$MDa = 1$			
	$\theta_{b,w}$	$Nu_{D,w}$	$\theta_{b,s}/Br$	$Nu_{D,s}$	$\theta_{b,w}$	$Nu_{D,w}$	$\theta_{b,s}/Br$	$Nu_{D,s}$
Panel a								
0.0001	0.9949	32.29	0.0006	1263	0.9948	33.54	0.0008	1136
0.0002	0.9921	26.43	0.0013	790.9	0.9919	25.96	0.0015	710.3
0.0005	0.9855	19.19	0.0030	437.9	0.9853	19.72	0.0037	384.4
0.001	0.9773	15.01	0.0059	279.7	0.9769	15.31	0.0071	245.2
0.002	0.9645	11.83	0.0111	179.5	0.9639	12.00	0.0137	155.9
0.005	0.9363	8.596	0.0255	100.9	0.9353	8.733	0.0317	86.42
0.01	0.9016	6.781	0.0468	65.91	0.9001	6.886	0.0589	55.73
0.02	0.8494	5.389	0.0840	43.55	0.8471	5.469	0.1075	36.33
0.05	0.7401	4.077	0.1736	25.82	0.7367	4.134	0.2289	21.16
0.1	0.6153	3.430	0.2872	17.85	0.6110	3.477	0.3889	14.50
0.2	0.4465	3.077	0.4504	12.79	0.4414	3.119	0.6254	10.40
0.5	0.1815	2.979	0.7135	9.214	0.1772	3.020	1.0102	7.620
1	0.0410	2.978	0.8537	8.190	0.0392	3.019	1.2126	6.852
2	0.0021	2.978	0.8925	7.964	1.91E−03	3.019	1.2673	6.687
5	2.75E−07	2.978	0.8945	7.952	2.23E−07	3.019	1.2701	6.679
∞	0	2.978	0.8945	7.952	0	3.019	1.2701	6.679
	$MDa = 0.1$				$MDa = 0.01$			
Panel b								
0.0001	0.9942	36.55	0.0019	725.2	0.9924	50.28	0.0119	395.4
0.0002	0.9910	29.39	0.0038	443.4	0.9882	37.63	0.0237	243.0
0.0005	0.9836	21.79	0.0092	236.4	0.9788	28.09	0.0586	125.7
0.001	0.9744	16.89	0.0181	146.9	0.9668	21.94	0.1160	78.29
0.002	0.9600	13.29	0.0353	91.15	0.9486	16.99	0.2288	49.64
0.005	0.9287	9.621	0.0847	48.97	0.9092	12.23	0.5566	28.46
0.01	0.8903	7.569	0.1625	31.01	0.8620	9.539	1.0788	19.57
0.02	0.8330	5.996	0.3078	20.06	0.7929	7.492	2.0572	14.05
0.05	0.7149	4.517	0.6940	11.91	0.6559	5.579	4.6266	9.663
0.1	0.5828	3.792	1.2305	8.527	0.5101	4.653	8.0839	7.657
0.2	0.4088	3.404	2.0434	6.554	0.3301	4.184	13.029	6.401
0.5	0.1508	3.304	3.3300	5.309	0.0964	4.083	19.859	5.612
1	0.0289	3.303	3.9428	4.997	0.0125	4.082	22.328	5.443
2	1.06E−03	3.303	4.0828	4.939	2.11E−04	4.082	22.691	5.421
5	5.28E−08	3.303	4.0882	4.937	1.02E−09	4.082	22.697	5.421
∞	0	3.303	4.0882	4.937	0	4.082	22.698	5.421
	$MDa = 0.001$				$MDa = 0.0001$			
Panel c								
0.0001	0.9896	71.12	0.1048	224.7	0.9868	89.10	1.0102	154.3
0.0002	0.9836	53.27	0.2087	146.3	0.9790	69.54	2.0115	115.8
0.0005	0.9711	36.74	0.5172	83.85	0.9630	45.71	4.9788	78.94
0.001	0.9555	28.81	1.0247	57.09	0.9444	34.33	9.8382	58.89
0.002	0.9321	21.96	2.0201	40.46	0.9172	25.49	19.324	44.19
0.005	0.8833	15.27	4.8941	26.81	0.8632	16.87	46.506	30.14
0.01	0.8272	11.59	9.4153	20.11	0.8036	12.46	88.937	22.58
0.02	0.7485	8.857	17.746	15.32	0.7226	9.34	166.55	17.02
0.05	0.6005	6.391	39.023	10.97	0.5740	6.647	362.94	11.99
0.1	0.4514	5.258	66.659	8.794	0.4267	5.457	615.26	9.514
0.2	0.2761	4.729	104.42	7.398	0.2561	4.923	954.96	7.954
0.5	0.0685	4.632	151.84	6.542	0.0598	4.834	1367.5	7.020
1	6.75E−03	4.632	166.01	6.379	5.33E−03	4.834	1482.5	6.850
2	6.58E−05	4.632	167.54	6.363	4.24E−05	4.834	1493.7	6.835
5	6.07E−11	4.632	167.56	6.363	2.14E−11	4.834	1493.8	6.835
∞	0	4.632	167.61	6.361	0	4.830	1504.0	6.802

these figures are the developing Nusselt number for different values of the aspect ratio, the Darcy number, and the Brinkman number. A detailed discussion concerning the behavior of these acquired tabulated data and graphical information is in the next section.

4. Results and discussion

The investigation of the frictional heating in the absence of a wall temperature change can be interesting, by its own. Fig. 2 shows the dimensionless bulk temperature $\theta_{b,s}(\bar{x})/Br$

Table 2
The bulk temperatures and the Nusselt numbers when $b/a = 2$, for (a) $MDa = \infty$ and 1, (b) $MDa = 0.1$ and 0.01, and (c) $MDa = 0.001$ and 0.0001

$\frac{x/a}{Pe}$	$MDa = \infty$				$MDa = 1$			
	$\theta_{b,w}$	$Nu_{D,w}$	$\theta_{b,s}/Br$	$Nu_{D,s}$	$\theta_{b,w}$	$Nu_{D,w}$	$\theta_{b,s}/Br$	$Nu_{D,s}$
Panel a								
0.0001	0.9964	42.07	0.0004	1942	0.9963	43.16	0.0005	1626
0.0002	0.9943	33.56	0.0008	1233	0.9942	34.50	0.0010	1027
0.0005	0.9897	24.03	0.0019	682.2	0.9894	24.66	0.0025	563.5
0.001	0.9838	19.10	0.0037	433.6	0.9834	19.57	0.0049	354.8
0.002	0.9746	15.08	0.0070	278.1	0.9739	15.47	0.0095	224.8
0.005	0.9541	10.97	0.0163	155.6	0.9529	11.23	0.0224	123.6
0.01	0.9285	8.676	0.0302	101.1	0.9268	8.880	0.0423	78.92
0.02	0.8894	6.896	0.0550	66.22	0.8869	7.053	0.0786	50.77
0.05	0.8057	5.195	0.1166	38.50	0.8016	5.309	0.1730	28.83
0.1	0.7063	4.325	0.1985	25.97	0.7007	4.418	0.3046	19.22
0.2	0.5640	3.788	0.3250	17.91	0.5568	3.873	0.5156	13.27
0.5	0.3079	3.483	0.5661	11.91	0.2997	3.567	0.9257	9.062
1	0.1173	3.405	0.7511	9.830	0.1115	3.489	1.2382	7.666
2	0.0174	3.393	0.8489	9.090	0.0158	3.476	1.3989	7.185
5	5.7E−05	3.392	0.8659	8.978	4.5E−05	3.476	1.4253	7.117
∞	0	3.392	0.8659	8.978	0	3.476	1.4254	7.116
	$MDa = 0.1$				$MDa = 0.01$			
Panel b								
0.0001	0.9958	49.08	0.0016	941.6	0.9944	64.89	0.0114	512.6
0.0002	0.9934	39.45	0.0032	583.6	0.9912	51.31	0.0227	313.5
0.0005	0.9879	28.25	0.0079	313.0	0.9840	37.85	0.0564	165.3
0.001	0.9811	22.09	0.0156	192.7	0.9750	28.97	0.1118	103.3
0.002	0.9704	17.55	0.0307	118.8	0.9613	22.58	0.2212	65.21
0.005	0.9467	12.69	0.0744	63.39	0.9312	16.32	0.5420	37.33
0.01	0.9175	9.998	0.1443	39.86	0.8947	12.67	1.0587	25.64
0.02	0.8733	7.914	0.2774	25.60	0.8407	9.905	2.0433	18.35
0.05	0.7798	5.929	0.6428	15.02	0.7307	7.279	4.7192	12.52
0.1	0.6712	4.922	1.1762	10.63	0.6087	5.963	8.5319	9.789
0.2	0.5195	4.322	2.0493	8.034	0.4469	5.202	14.522	8.011
0.5	0.2595	4.008	3.7083	6.279	0.1937	4.835	24.916	6.743
1	0.0853	3.930	4.8690	5.726	0.0505	4.754	31.029	6.358
2	0.0094	3.917	5.3801	5.554	0.0035	4.743	33.053	6.259
5	1.3E−05	3.917	5.4435	5.535	1.2E−06	4.743	33.203	6.252
∞	0	3.917	5.4436	5.535	0	4.743	33.205	6.252
	$MDa = 0.001$				$MDa = 0.0001$			
Panel c								
0.0001	0.9922	87.03	0.1035	295.3	0.9902	105.0	1.0088	181.5
0.0002	0.9879	69.16	0.2065	188.9	0.9849	85.74	2.0127	137.8
0.0005	0.9784	50.01	0.5131	109.4	0.9732	60.23	4.9978	97.45
0.001	0.9665	38.59	1.0188	75.38	0.9592	45.55	9.9079	74.70
0.002	0.9487	29.03	2.0157	53.54	0.9386	33.47	19.550	56.82
0.005	0.9115	20.25	4.9217	35.39	0.8973	22.28	47.509	39.04
0.01	0.8680	15.28	9.5611	26.46	0.8510	16.37	91.891	29.28
0.02	0.8063	11.57	18.293	20.02	0.7871	12.12	174.99	21.98
0.05	0.6868	8.200	41.570	14.13	0.6664	8.462	395.16	15.26
0.1	0.5602	6.592	73.979	11.12	0.5404	6.775	699.73	11.87
0.2	0.3987	5.713	123.52	9.089	0.3810	5.875	1161.7	9.631
0.5	0.1591	5.316	205.08	7.650	0.1480	5.477	1909.8	8.065
1	0.0362	5.236	248.51	7.234	0.0322	5.400	2295.1	7.623
2	0.0019	5.228	260.73	7.140	0.0016	5.392	2397.8	7.528
5	2.8E−07	5.228	261.41	7.135	1.7E−07	5.392	2403.0	7.523
∞	0	5.227	261.81	7.127	0	5.392	2426.2	7.473

plotted when $b/a = 1$, for different MDa parameters. This figure illustrates the dimensionless bulk temperature due to the frictional heating in the thermally developing region within a square channel. One can observe that increasing MDa decreases the dimensionless bulk temperature. For the same aspect ratio and MDa parameters, the Nusselt number $Nu_{D,s}$ is presented in Fig. 3. As can be seen from Eq. (27), $Nu_{D,s}$ does not depend on Br, in the developing

Table 3
The bulk temperatures and the Nusselt numbers when $b/a = 4$, for (a) $MDa = \infty$ and 1, (b) $MDa = 0.1$ and 0.01, and (c) $MDa = 0.001$ and 0.0001

$\frac{x/a}{Pe}$	$MDa = \infty$				$MDa = 1$			
	$\theta_{b,w}$	$Nu_{D,w}$	$\theta_{b,s}/Br$	$Nu_{D,s}$	$\theta_{b,w}$	$Nu_{D,w}$	$\theta_{b,s}/Br$	$Nu_{D,s}$
Panel a								
0.0001	0.9970	50.25	0.0003	2703	0.9969	49.12	0.0005	2215
0.0002	0.9953	40.73	0.0006	1719	0.9952	41.04	0.0009	1371
0.0005	0.9913	29.64	0.0016	951.6	0.9911	30.55	0.0022	749.9
0.001	0.9863	23.40	0.003	608.2	0.9860	24.03	0.0042	475.6
0.002	0.9784	18.35	0.0058	390.7	0.9779	18.82	0.0082	301.9
0.005	0.9609	13.53	0.0134	218.3	0.9600	13.84	0.0193	165.2
0.01	0.9388	10.78	0.0248	141.6	0.9373	11.03	0.0366	105.2
0.02	0.9044	8.628	0.0453	92.59	0.9023	8.818	0.0683	67.36
0.05	0.8294	6.596	0.0965	53.42	0.8259	6.732	0.1519	37.89
0.1	0.7378	5.574	0.1657	35.61	0.7330	5.687	0.2705	24.99
0.2	0.6019	4.989	0.2753	24.11	0.5954	5.094	0.4652	17.04
0.5	0.3433	4.687	0.4942	15.63	0.3353	4.799	0.8593	11.50
1	0.1394	4.563	0.6725	12.72	0.1331	4.681	1.1768	9.677
2	0.0239	4.481	0.7756	11.63	0.0218	4.603	1.3554	9.013
5	1.3E−04	4.442	0.7971	11.44	1.0E−04	4.566	1.3907	8.901
∞	0	4.441	0.7973	11.43	0	4.564	1.3908	8.901
	$MDa = 0.1$				$MDa = 0.01$			
Panel b								
0.0001	0.9964	54.81	0.0015	1209	0.9949	72.91	0.0112	653.2
0.0002	0.9945	45.51	0.0030	726.6	0.9925	57.24	0.0222	389.0
0.0005	0.9899	34.60	0.0074	382.2	0.9867	44.38	0.0552	198.0
0.001	0.9841	27.33	0.0146	236.8	0.9792	35.46	0.1098	122.8
0.002	0.9749	21.40	0.0288	146.9	0.9674	27.78	0.2177	78.18
0.005	0.9548	15.50	0.0701	78.15	0.9417	19.76	0.5349	45.06
0.01	0.9296	12.33	0.1366	48.99	0.9105	15.41	1.0486	30.94
0.02	0.8909	9.821	0.2640	31.43	0.8637	12.12	2.0348	22.16
0.05	0.8077	7.434	0.6179	18.44	0.7665	8.951	4.7546	15.14
0.1	0.7082	6.251	1.1432	13.07	0.6553	7.392	8.7185	11.86
0.2	0.5637	5.594	2.0224	9.923	0.5013	6.542	15.153	9.728
0.5	0.2995	5.297	3.7647	7.826	0.2396	6.182	27.062	8.225
1	0.1078	5.187	5.0722	7.157	0.0727	6.058	34.909	7.752
2	0.0145	5.116	5.7201	6.930	0.0069	5.982	38.049	7.609
5	3.7E−05	5.081	5.8212	6.899	6.4E−06	5.949	38.383	7.595
∞	0	5.080	5.8215	6.898	0	5.947	38.386	7.594
	$MDa = 0.001$				$MDa = 0.0001$			
Panel c								
0.0001	0.9931	100.7	0.1009	363.7	0.9912	129.9	0.952	243.1
0.0002	0.9897	77.41	0.2033	227.2	0.9868	99.12	1.955	174.9
0.0005	0.9821	58.33	0.5091	128.4	0.9776	69.33	4.945	117.1
0.001	0.9723	46.08	1.014	88.50	0.9661	53.72	9.875	88.51
0.002	0.9572	35.39	2.013	63.43	0.9489	40.16	19.59	67.28
0.005	0.9255	24.37	4.936	42.32	0.9140	26.64	47.92	46.39
0.01	0.8885	18.45	9.635	31.67	0.8747	19.65	93.26	34.8.0
0.02	0.8350	14.03	18.57	24.00	0.8193	14.66	179.1	26.16
0.05	0.7294	9.969	42.82	16.93	0.7123	10.25	411.0	18.17
0.1	0.6138	8.069	77.53	13.31	0.5969	8.259	741.3	14.12
0.2	0.4589	7.085	132.7	10.88	0.4432	7.253	1264	11.45
0.5	0.2064	6.691	231.0	9.161	0.1955	6.857	2182	9.579
1	0.0567	6.558	291.1	8.637	0.0520	6.723	2731	9.019
2	0.0045	6.480	312.4	8.493	0.0038	6.644	2918	8.869
5	2.3E−06	6.449	314.3	8.481	1.6E−06	6.615	2933	8.858
∞	0	6.443	315.1	8.465	0	6.608	2953	8.815

region. However, $MDa = 0.1$ serves as a threshold value beyond which $Nu_{D,s}$ increases as MDa increases and it decreases as $\bar{x}$ increases. For the smaller values of MDa, one observes intersections at some stream-wise locations in such a way that $Nu_{D,s}$ increases with a decrease in MDa within and near the thermally fully developed region. Also, it is to be noted that the curves for $MDa = 1$ and $MDa = \infty$ are very close to each other and act in a similar

Table 4
The bulk temperatures and the Nusselt numbers when $b/a = 10$, for (a) $MDa = \infty$ and 1, (b) $MDa = 0.1$ and 0.01, and (c) $MDa = 0.001$ and 0.0001

$\frac{x/a}{Pe}$	$MDa = \infty$				$MDa = 1$			
	$\theta_{b,w}$	$Nu_{D,w}$	$\theta_{b,s}/Br$	$Nu_{D,s}$	$\theta_{b,w}$	$Nu_{D,w}$	$\theta_{b,s}/Br$	$Nu_{D,s}$
Panel a								
0.0001	0.9970	55.09	0.0003	3621	0.9969	56.12	0.0004	2865
0.0002	0.9955	45.36	0.0006	2255	0.9954	46.21	0.0008	1766
0.0005	0.9921	33.54	0.0014	1233	0.9919	34.21	0.002	952.4
0.001	0.9876	26.89	0.003	781.9	0.9873	27.40	0.004	596.7
0.002	0.9805	21.58	0.005	499.7	0.9801	22.00	0.008	375.9
0.005	0.9644	16.09	0.012	279.4	0.9637	16.40	0.018	205.5
0.01	0.9439	12.87	0.022	181.5	0.9427	13.12	0.034	130.9
0.02	0.9118	10.36	0.041	118.6	0.9102	10.55	0.063	83.73
0.05	0.8408	8.035	0.087	68.19	0.8381	8.159	0.141	46.90
0.1	0.7522	6.905	0.150	45.19	0.7486	7.006	0.253	30.79
0.2	0.6173	6.318	0.251	30.35	0.6126	6.410	0.438	20.92
0.5	0.3525	6.112	0.455	19.58	0.3468	6.207	0.816	14.16
1	0.1407	6.041	0.621	15.98	0.1364	6.141	1.120	11.99
2	0.0228	5.989	0.714	14.68	0.0215	6.092	1.287	11.23
3	0.0038	5.965	0.729	14.50	0.0034	6.070	1.314	11.12
4	6.2E−04	5.951	0.731	14.47	5.5E−04	6.057	1.318	11.11
5	1.0E−04	5.942	0.732	14.46	8.7E−05	6.048	1.319	11.10
∞	0	5.908	0.732	14.46	0	6.016	1.319	11.10
	$MDa = 0.1$				$MDa = 0.01$			
Panel b								
0.0001	0.9963	62.53	0.0015	1491	0.9947	84.63	0.011	749.9
0.0002	0.9946	51.14	0.0029	893.3	0.9925	64.89	0.022	449.6
0.0005	0.9907	38.25	0.0071	463.6	0.9875	49.21	0.055	228.6
0.001	0.9856	30.41	0.014	282.6	0.9811	38.92	0.109	140.8
0.002	0.9776	24.41	0.028	172.8	0.9710	30.76	0.216	88.70
0.005	0.9595	18.16	0.068	91.44	0.9484	22.64	0.531	50.89
0.01	0.9365	14.50	0.132	57.43	0.9203	17.89	1.044	35.16
0.02	0.9008	11.60	0.257	36.90	0.8776	14.12	2.032	25.36
0.05	0.8233	8.859	0.603	21.70	0.7877	10.49	4.778	17.44
0.1	0.7286	7.556	1.123	15.43	0.6828	8.754	8.828	13.72
0.2	0.5872	6.886	2.001	11.79	0.5329	7.873	15.51	11.33
0.5	0.3187	6.672	3.768	9.419	0.2655	7.600	28.25	9.688
1	0.1168	6.610	5.118	8.685	0.0847	7.530	37.02	9.185
2	0.0159	6.565	5.799	8.439	0.0088	7.480	40.72	9.033
5	4.2E−05	6.525	5.906	8.405	1.0E−05	7.437	41.15	9.016
∞	0	6.495	5.907	8.405	0	7.399	41.15	9.016
	$MDa = 0.001$				$MDa = 0.0001$			
Panel c								
0.0001	0.9932	117.7	0.133	303.1	0.9916	154.8	1.085	243.2
0.0002	0.9902	88.08	0.235	218.3	0.9876	115.5	2.089	189.3
0.0005	0.9836	64.67	0.541	134.5	0.9794	78.16	5.083	131.1
0.001	0.9752	50.49	1.046	95.13	0.9694	59.57	10.03	99.23
0.002	0.9624	38.97	2.047	68.95	0.9546	44.35	19.79	75.12
0.005	0.9347	27.63	4.987	46.69	0.9243	30.03	48.38	51.80
0.01	0.9015	21.15	9.734	35.41	0.8892	22.40	94.36	39.07
0.02	0.8531	16.14	18.80	27.08	0.8392	16.79	181.9	29.52
0.05	0.7559	11.57	43.69	19.25	0.7407	11.87	421.3	20.60
0.1	0.6467	9.477	79.86	15.21	0.6314	9.680	767.8	16.08
0.2	0.4953	8.444	138.5	12.51	0.4809	8.625	1327	13.11
0.5	0.2347	8.145	246.8	10.64	0.2242	8.327	2349	11.07
1	0.0689	8.070	316.9	10.08	0.0641	8.251	2997	10.47
2	0.0061	8.018	343.7	9.919	0.0053	8.198	3236	10.31
3	5.4E−04	7.995	346.0	9.906	4.5E−04	8.175	3256	10.29
4	4.8E−05	7.982	346.2	9.905	3.8E−05	8.161	3258	10.29
5	4.3E−06	7.973	346.3	9.905	3.2E−06	8.153	3258	10.29
∞	0	7.931	347.0	9.890	0	8.151	3268	10.27

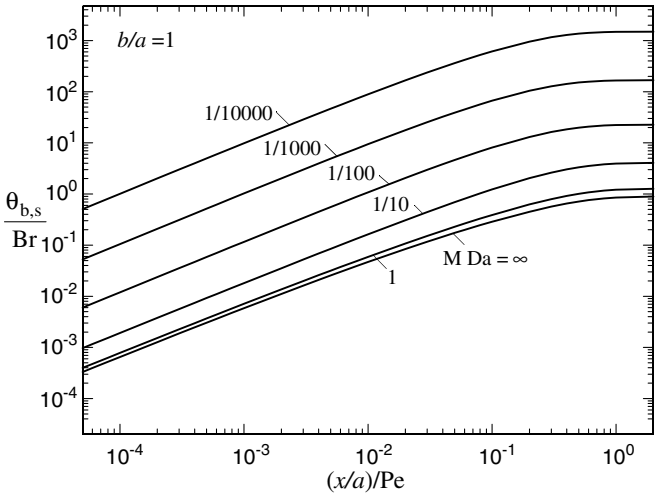

Fig. 2. The bulk temperature due to the frictional heating in the thermally developing region within a square channel.

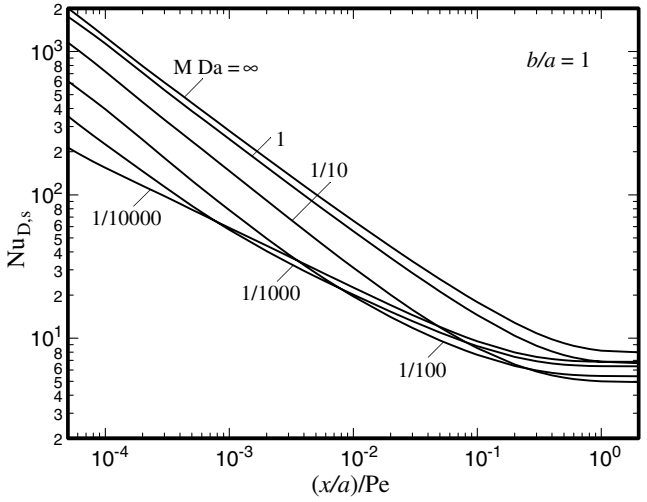

Fig. 3. The Nusselt number due to the frictional heating in the thermally developing region within a square channel.

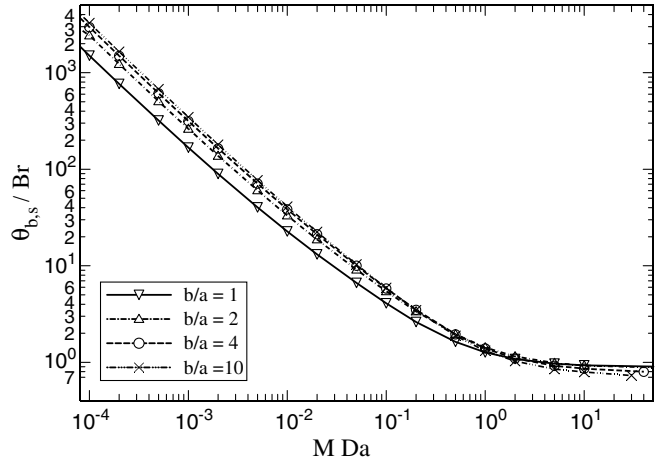

Fig. 4. The variation of frictional heating induced bulk temperature as a function of *MDa* under thermally fully developed condition for ducts with different aspect ratios.

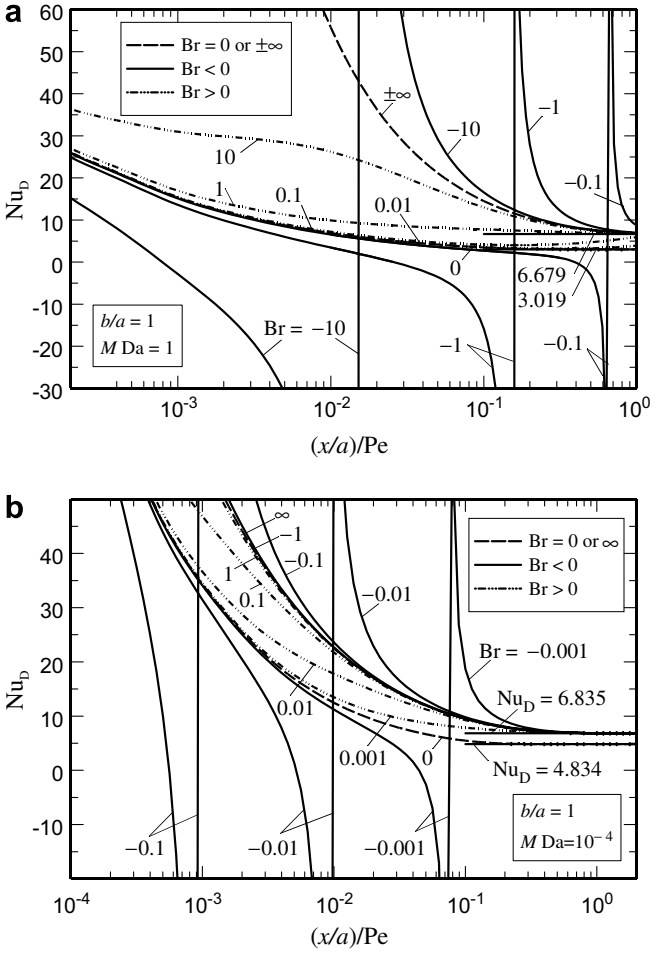

Fig. 5. The Nusselt number in the thermal entrance region when $b/a = 1$; (a) for $MDa = 1$ and (b) for $MDa = 10^{-4}$.

manner in both Figs. 2 and 3. It is possible that this unique $Nu_{D,s}$ trend is a result of changes in the velocity distribution. Additionally, the *MDa* values of near 1 simulate hyperporous media for those the boundary effects are present even in the duct center. For small values of *MDa*, there is a thin near wall region in which the velocity changes are present and out of this region there exists the core region as reported in [16].

Fig. 4 shows the variation of frictional heating induced bulk temperature $\theta_{b,s}(\bar{x})/Br$ as a function of *MDa* under thermally fully developed condition for ducts with different aspect ratios. One notes an intersection that occurs in $MDa \cong 1.5$; beyond which, the dimensionless bulk temperature decreases with the duct aspect ratio. However, for smaller values of *MDa* the converse is true.

To illustrate the combined effects, Figs. 5–8 show the Nusselt number in the developing region for some *Br* values. Each figure covers two distinct value of $MDa = 10^{-4}$ and 1 where the latter simulates a hyperporous medium. As a common trend in all of these figures, one observes that the negative values of *Br* will lead to a jump in the Nusselt number plots and this is similar to what previously reported in the literature for parallel plate channel or circu-

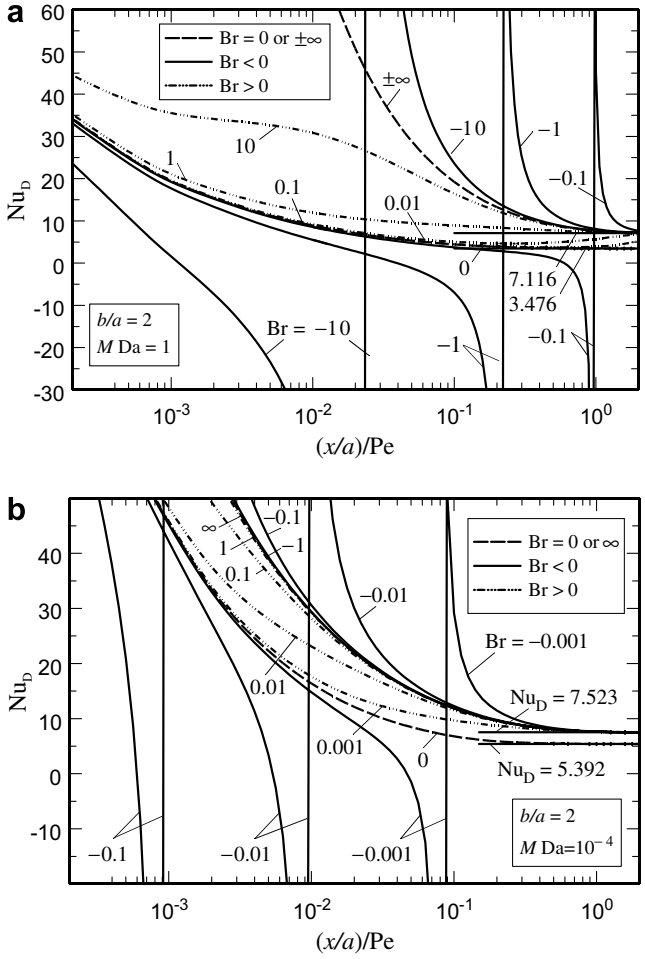

Fig. 6. The Nusselt number in the thermal entrance region when $b/a = 2$; (a) for $MDa = 1$ and (b) for $MDa = 10^{-4}$.

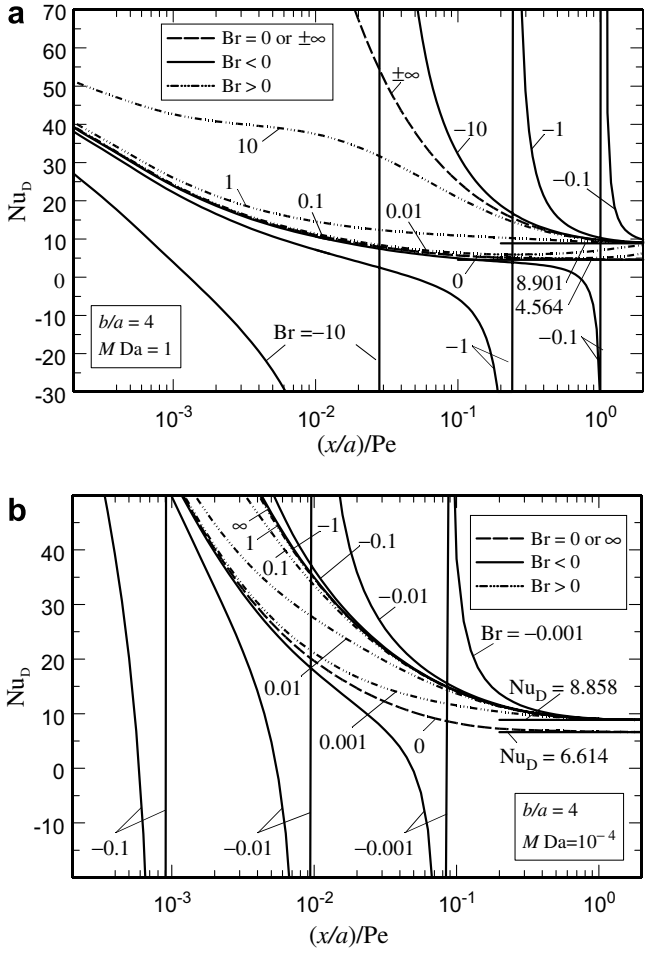

Fig. 7. The Nusselt number in the thermal entrance region when $b/a = 4$; (a) for $MDa = 1$ and (b) for $MDa = 10^{-4}$.

lar tubes. Another similar behavior is that $Nu_{D,s}$ values computed with both positive and negative Br will merge to a single Nusselt number in the fully developed region that is independent of the Brinkman number. A quick check of these figures shows that, with non-zero Br values, the fully developed Nusselt number is higher than the case when there is no dissipation, regardless of the sign or the value of Br.

It is interesting that for the limiting values of $Br = \pm\infty$, the Nusselt number plots are not different in the developing region. However, the mathematical value of this limiting Br changes with MDa in such a way that for $MDa = 10^{-4}$ even $Br = 1$ is large enough to be almost indistinguishable from that of $Br = -1$ while when $MDa = 1$, the absolute value of this limiting Br is higher than $Br = 10$.

Comparing these figures for different aspect ratios, it is found that, for a fixed MDa value, the stream-wise location of the point where the jump occurs is nearly independent of the cross-section geometry. This can be also verified by comparing these data, for example, with those in [2, Fig. 7] and in [9, Fig. 5]. It is also interesting to note that the $Br = -10$ with $MDa = 1$ leads to a jump at $\bar{x} \cong 0.015$ which is close to approximate values of 0.015 and 0.03 reported in [9,2], respectively. This fact drives home the point that the jump location is almost independent of the duct cross-section. Another point worthy of noting is that increasing MDa and the aspect ratio as well as decreasing Br will increase the thermal entry length.

Fig. 9 shows the variation of the fully developed Nusselt number as a function of MDa for ducts with different aspect ratios. Regardless of the b/a value, the maximum $Nu_{D,s}$ is associated with the highest MDa value and the minimum $Nu_{D,s}$ occurs at $MDa \cong 0.1$. As MDa approaches zero the data asymptotically approach those of slug flow, as shown in Fig. 9. Then, the Nusselt number begins to reduce, going through a minimum, shows a relatively large increase, and asymptotically approaches the Nusselt number for clear fluid through the same passage. As the aspect ratio plunges the difference between the Nusselt numbers for the clear fluid and that of the slug flow decreases. This minimum point, already highlighted in Fig. 3 as a threshold value, if arranged as $3\sqrt{MK} \cong a$, can be interpreted as the limit value where the macro and micro length scales (see for example [33]) merge to each other. This is something similar to what previously reported by Hooman and Gurgenci [5] for flow through a parallel plate porous channel.

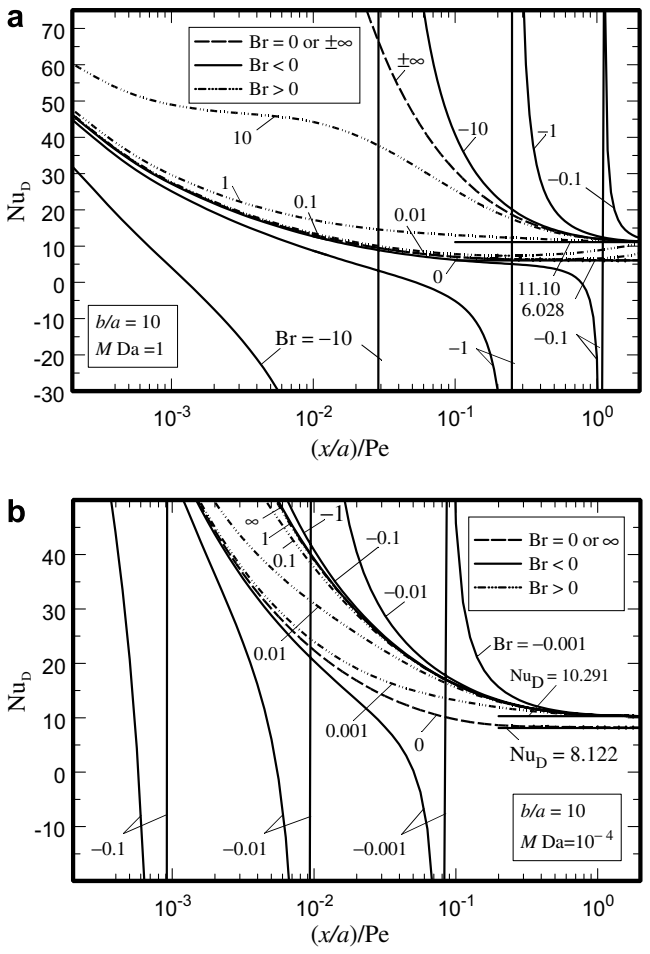

Fig. 8. The Nusselt number in the thermal entrance region when $b/a = 10$; (a) for $MDa = 1$ and (b) for $MDa = 10^{-4}$.

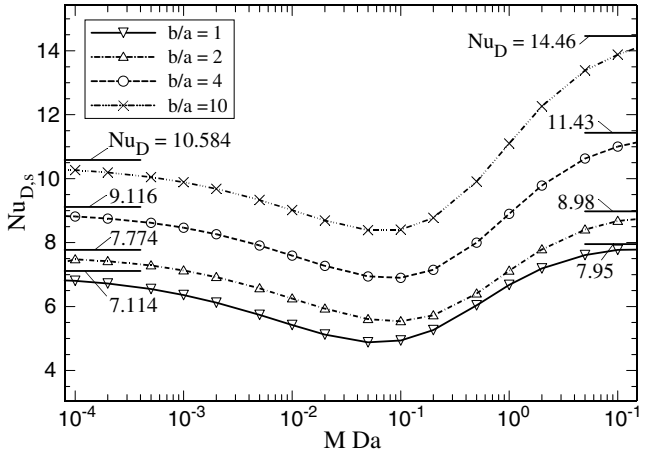

Fig. 9. The variation of the Nusselt number heating induced bulk temperature as a function of MDa under thermally fully developed condition for ducts with different aspect ratios.

The data presented in Tables 1–4 are a sample of the data gathered for preparing the figures. Each table shows the dimensionless bulk temperature and the local Nusselt number for the two parts of our combined problem versus $\bar{x}$. The error in these data is generally due to the truncation error although a larger error is expected at very small $\bar{x}$ values. A relatively large number of basis functions are used in order to reduce the errors; especially, for small values of $\bar{x}$ similar to [18]. The data for $\theta_{b,w}$ and $Nu_{D,w}$ behave similar to those in [18], as expected. Also, the effect of the combined Nusselt numbers approaches available data for $Nu_{D,w}$ and $Nu_{D,s}$ as $\hat{x} \to 0$ and as $\hat{x} \to \infty$, respectively.

5. Conclusion

The Extended Weighted Residuals Method (EWRM) is applied to investigate a thermally developing Brinkman–Brinkman forced convection problem through a duct of rectangular cross-section occupied by a fluid-saturated porous medium. This problem is decomposed into two different ones with different physical interpretation. For one of these two problems, as well as the combined one, it is found that $MDa = 0.1$ is a threshold value. For the combined problem, it is observed that increasing MDa and b/a, as well as decreasing Br will increase the thermal development length. Moreover, the fully developed Nusselt number with non-zero Br is found to be higher than the case when there is no dissipation, regardless of the sign or value of Br. For the fully developed Nusselt number, which is independent of Br, it is observed that as b/a decreases the difference between the Nusselt numbers for the clear fluid and that of the slug flow also decreases. Besides, it was concluded that the jump in Nu_D plots for the case of negative Br happens at some longitudinal locations, which is nearly independent of the duct geometry but dependent on the MDa value.

Acknowledgement

The first author, the scholarship holder, acknowledges the support provided by The University of Queensland in terms of UQILAS, Endeavor IPRS, and School Scholarship.

References

[1] D.A. Nield, A. Bejan, Convection in Porous Media, third ed., Springer, New York, 2006.
[2] A. Haji-Sheikh, W.J. Minkowycz, E.M. Sparrow, Green's function solution of temperature field for flow in porous passages, Int. J. Heat Mass Transfer 47 (2004) 4685–4695.
[3] D.A. Nield, A.V. Kuznetsov, M. Xiong, Thermally developing forced convection in a porous medium: parallel plate channel with walls at uniform temperature with axial conduction and viscous dissipation effects, Int. J. Heat Mass Transfer 46 (2003) 643–651.
[4] K. Hooman, M. Gorji-Bandpy, Laminar dissipative flow in a porous channel bounded by isothermal parallel plates, Appl. Math. Mech. English Ed. 26 (2005) 578–593.
[5] K. Hooman, H. Gurgenci, Effects of viscous dissipation and boundary conditions on forced convection in a channel occupied by a saturated porous medium, Transport Porous Media, doi:10.1007/s11242-006-9049-4.
[6] A.V. Kuznetsov, D.A. Nield, M. Xiong, Thermally developing forced convection in a porous medium: circular ducts with walls at constant

temperature, with longitudinal conduction and viscous dissipation effects, Transport Porous Media 53 (2003) 331–345.
[7] A.A. Ranjbar-Kani, K. Hooman, Viscous dissipation effects on thermally developing forced convection in a porous medium: circular duct with isothermal wall, Int. Commun. Heat Mass Transfer 31 (2004) 897–907.
[8] K. Hooman, A. Pourshaghaghy, A. Ejlali, Effects of viscous dissipation on thermally developing forced convection in a porous saturated circular tube with an isoflux wall, Appl. Math. Mech. English Ed. 27 (2006) 617–626.
[9] A. Haji-Sheikh, W.J. Minkowycz, E.M. Sparrow, A numerical study of the heat transfer to fluid flow through circular porous passages, Numer. Heat Transfer A 46 (2004) 929–955.
[10] D.A. Nield, A note on a Brinkman–Brinkman forced convection problem, Transport Porous Media 64 (2006) 185–188.
[11] H.C. Brinkman, On the permeability of media consisting of closely packed porous particles, Appl. Sci. Res. A 1 (1947) 81–86.
[12] H.C. Brinkman, Heat effects in capillary flow, Appl. Sci. Res. A 2 (1951) 120–124.
[13] K. Hooman, Fully developed temperature distribution in porous saturated duct of elliptical cross-section, with viscous dissipation effects and entropy generation analysis, Heat Transfer Res. 36 (2005) 237–245.
[14] A. Haji-Sheikh, Fully developed heat transfer to fluid flow in rectangular passages filled with porous materials, ASME J. Heat Transfer 128 (2006) 550–556.
[15] K. Hooman, H. Gurgenci, Effects of temperature-dependent viscosity variation on entropy generation, heat, and fluid flow through a porous-saturated duct of rectangular cross-section, Appl. Math. Mech. Eng. Ed. 28 (2007) 69–78.
[16] K. Hooman, A.A. Merrikh, Analytical solution of forced convection in a duct of rectangular cross-section saturated by a porous medium, ASME J. Heat Transfer 128 (2006) 596–600.
[17] A. Haji-Sheikh, K. Vafai, Analysis of flow and heat transfer in porous media imbedded inside various-shaped ducts, Int. J. Heat Mass Transfer 47 (2004) 1889–1905.
[18] A. Haji-Sheikh, D.A. Nield, K. Hooman, Heat transfer in the thermal entrance region for flow through rectangular porous passages, Int. J. Heat Mass Transfer 49 (2006) 3004–3015.
[19] A. Haji-Sheikh, E.M. Sparrow, W.J. Minkowycz, Heat transfer to flow through porous passages using extended weighted residuals method – a Green's function solution, Int. J. Heat Mass Transfer 48 (2005) 1330–1349.
[20] R.K. Shah, A.L. London, Laminar Flow Forced Convection in Ducts Advances in Heat Transfer, Supplement 1, Academic Press, New York, 1978.
[21] J.V. Beck, K. Cole, A. Haji-Sheikh, B. Litkouhi, Heat Conduction Using Green's Functions, Hemisphere Publ. Corp, Washington, DC, 1992.
[22] E. Magyari, D.A.S. Rees, B. Keller, Effect of viscous dissipation on the flow in fluid saturated porous media, in: K. Vafai (Ed.), Handbook of Porous Media, second ed., Taylor and Francis, New York, 2005, pp. 373–407.
[23] A.K. Al-Hadhrami, L. Elliot, D.B. Ingham, A new model for viscous dissipation in porous media across a range of permeability values, Transport Porous Media 53 (2003) 117–122.
[24] D.A. Nield, Resolution of a paradox involving viscous dissipation and nonlinear drag in a porous medium, Transport Porous Media 41 (2000) 349–357.
[25] D.A. Nield, Modelling fluid flow in saturated porous media and at interfaces, in: D.B. Ingham, I. Pop (Eds.), Transport Phenomena in Porous Media II, Elsevier Science, Oxford, 2002.
[26] D.A. Nield, Comments on A new model for viscous dissipation in porous media across a range of permeability values, Transport Porous Media 55 (2004) 253–254.
[27] K. Hooman, A. Ejlali, Second law analysis of laminar flow in a channel filled with saturated porous media: a numerical solution, Entropy 7 (2005) 300–307.
[28] K. Hooman, A.A. Merrikh, A. Ejlali, Comments on "Flow, thermal, and entropy generation characteristics inside a porous channel with viscous dissipation" by S. Mahmud and R.A. Fraser, Int. J. Thermal Sciences 44 (2005) 21–32. Int. J. Thermal Sciences, doi:10.1016/j.ijthermalsci.2007.01.001.
[29] K. Hooman, Second law analysis of thermally developing forced convection in a porous medium, Heat Transfer Research 36 (2005) 437–447.
[30] K. Hooman, A. Ejlali, Entropy generation for forced convection in a porous saturated circular tube with uniform wall temperature, Int. Comm. in Heat and Mass Transfer, doi:10.1016/j.icheatmasstransfer.2006.10.008.
[31] K. Hooman, H. Gurgenci, A.A. Merrikh, Heat transfer and entropy generation optimization of forced convection in a porous-saturated duct of rectangular cross-section, Heat Mass Transfer, doi:10.1016/j.ijheatmasstransfer.2006.11.015.
[32] W.P. Breugem, D.A.S. Rees, A derivation of the volume-averaged Boussinesq equations for flow in porous media with viscous dissipation, Transport Porous Media 63 (2006) 1–12.
[33] D.A. Nield, A.V. Kuznetsov, Forced convection in porous media: transverse heterogeneity effects and thermal development, in: K. Vafai (Ed.), Handbook of Porous Media, second ed., Taylor and Francis, New York, 2005, pp. 143–193.